



## The role of input chirp on phase shifters based on slow and fast light effects in semiconductor optical amplifiers

Xue, Weiqi; Chen, Yaohui; Öhman, Filip; Mørk, Jesper

*Published in:*  
Optics Express

*Link to article, DOI:*  
[10.1364/OE.17.001404](https://doi.org/10.1364/OE.17.001404)

*Publication date:*  
2009

*Document Version*  
Publisher's PDF, also known as Version of record

[Link back to DTU Orbit](#)

### *Citation (APA):*

Xue, W., Chen, Y., Öhman, F., & Mørk, J. (2009). The role of input chirp on phase shifters based on slow and fast light effects in semiconductor optical amplifiers. *Optics Express*, 17(3), 1404-1413. <https://doi.org/10.1364/OE.17.001404>

---

### General rights

Copyright and moral rights for the publications made accessible in the public portal are retained by the authors and/or other copyright owners and it is a condition of accessing publications that users recognise and abide by the legal requirements associated with these rights.

- Users may download and print one copy of any publication from the public portal for the purpose of private study or research.
- You may not further distribute the material or use it for any profit-making activity or commercial gain
- You may freely distribute the URL identifying the publication in the public portal

If you believe that this document breaches copyright please contact us providing details, and we will remove access to the work immediately and investigate your claim.

# The role of input chirp on phase shifters based on slow and fast light effects in semiconductor optical amplifiers

WeiQi Xue\*, Yaohui Chen, Filip Öhman, and Jesper Mørk

DTU Fotonik, Dept. of Photonics Engineering, Technical University of Denmark, Build. 343, DK-2800 Kongens Lyngby, Denmark  
[wexu@fotonik.dtu.dk](mailto:wexu@fotonik.dtu.dk)

**Abstract:** We experimentally investigate the initial chirp dependence of slow and fast light effects in a semiconductor optical amplifier followed by an optical filter. It is shown that the enhancement of the phase shift due to optical filtering strongly depends on the chirp of the input optical signal. We demonstrate  $\sim 120^\circ$  phase delay as well as  $\sim 170^\circ$  phase advance at a microwave frequency of 19 GHz for different optimum values of the input chirp. The experimental results are shown to be in good agreement with numerical results based on a four-wave mixing model. Finally, a simple physical explanation based on an analytical perturbative approach is presented.

©2009 Optical Society of America

**OCIS codes:** (230.4320) Nonlinear optical devices; (130.5990) Semiconductor; (070.6020) Signal processing

---

## References and links

1. L. V. Hau, S. E. Harris, Z. Dutton, and C. H. Behroozi, "Light speed reduction to 17 metres per second in an ultracold atomic gas," *Nature* **397**, 594-598 (1999).
2. M. S. Bigelow, N. N. Lepeshkin, and R. W. Boyd, "Superluminal and slow light propagation in a room-temperature solid," *Science* **301**, 200-202 (2003).
3. P. C. Ku, F. Sedgwick, C. J. Chang-Hasnain, P. Palinginis, T. Li, H. -L. Wang, S. -W. Chang and S. -L. Chuang, "Slow light in semiconductor quantum wells," *Opt. Lett.* **29**, 2291-2293 (2004).
4. Y. A. Vlasov, M. O'Boyle, H. F. Hamann, and S. J. McNab, "Active control of slow light on a chip with photonic crystal waveguides," *Nature* **438**, 65-69 (2005).
5. N. V. Jespersen, and P. R. Herczfeld, "Optical techniques for reconfiguring microwave phased arrays," *IEEE Trans. Antennas Propag.* **38**, 1054-1058 (1990).
6. J. Capmany, B. Ortega, D. Pastor, and S. Sales, "Discrete-time optical processing of microwave signals," *J. Lightwave Technol.* **25**, 702-723 (2005).
7. J. Mørk, R. Kjær, M. van der Poel, and K. Yvind, "Slow light in a semiconductor waveguide at gigahertz frequencies," *Opt. Express* **13**, 8136-8145 (2005).
8. H. Su, and S. L. Chuang, "Room-temperature slow light with semiconductor quantum-dot devices," *Opt. Lett.* **31**, 271-273 (2006).
9. C. J. Chang-Hasnain, and S. L. Chuang, "Slow and fast light in semiconductor quantum-well and quantum-dot devices," *J. Lightwave Technol.* **24**, 4642-4654 (2006).
10. P. K. Kondratko and S. L. Chuang, "Slow-to-fast light using absorption to gain switching in quantum-well semiconductor optical amplifier," *Opt. Express* **15**, 9963-9969 (2007).
11. F. Öhman, K. Yvind, and J. Mørk, "Voltage-controlled slow light in an integrated semiconductor structure with net gain," *Opt. Express* **14**, 9955-9962 (2006).
12. F. G. Sedgwick, B. Pesala, A. V. Uskov, and C. J. Chang-Hasnain, "Chirp-enhanced fast light in semiconductor optical amplifiers," *Opt. Express* **15**, 17631-17638 (2007).
13. J. Mørk, F. Öhman, M. van der Poel, Y. Chen, P. Lunnemann, and K. Yvind, "Slow and fast light: controlling the speed of light using semiconductor waveguides," *Laser Photonics Rev.* **2**, (2008) (to be published).
14. F. Öhman, K. Yvind, and J. Mørk, "Slow light in a semiconductor waveguide for true-time delay applications in microwave photonics," *IEEE Photon. Technol. Lett.* **19**, 1145-1147 (2007).
15. W. Xue, Y. Chen, F. Öhman, S. Sales, and J. Mørk, "Enhancing light slow-down in semiconductor optical amplifiers by optical filtering," *Opt. Lett.* **33**, 1084-1086 (2008).
16. H. Su, P. K. Kondratko, and S. L. Chuang, "Variable optical delay using population oscillation and four-wave-mixing in semiconductor optical amplifiers," *Opt. Express* **14**, 4800-4807 (2006).

17. M. S. Bigelow, N. N. Lepeshkin, and R. W. Boyd, "Observation of ultraslow light propagation in a ruby crystal at room temperature," *Phys. Rev. Lett.* **90**, 113903-1-4 (2003)
18. F. Koyama, and K. Iga, "Frequency chirping in external modulators," *J. Lightwave Technol.* **6**, 87-93 (1988)
19. G. H. Smith, D. Novak, and Z. Ahmed, "Overcoming chromatic-dispersion effects in fiber-wireless systems incorporating external modulators," *IEEE Trans. Microwave Theory Tech.* **45**, 1410-1415 (1997)
20. A. V. Uskov, and C. J. Chang-Hasnain, "Slow and superluminal light in semiconductor optical amplifiers," *Electron. Lett.* **41**, 55-56 (2005)
21. W. Xue, S. Sales, J. Mørk, and J. Capmany, "Widely tunable microwave photonic notch filter based on slow and fast light effects," *IEEE Photon. Technol. Lett.*, DOI: 10.1109/LPT.2008.2009468 (to be published)

---

## 1. Introduction

The demonstrations of slow and fast light effects in ultracold atomic gasses [1], various crystals [2], semiconductors [3], and photonic crystal waveguides [4] have stimulated extensive research on the physics and possible applications of these fascinating effects. Because of the ability to realize large phase or time shifts in a compact device, slow and fast light effects have the potential to be applied in microwave photonics, especially phased array antennas [5] and microwave photonic filters [6]. From the view of practical applications, due to the compact size, ease of integration, operation at room temperature and communication wavelengths, semiconductor waveguides are attractive and many promising results have already been reported [7-13]. Currently much work has focused on increasing the magnitude of the phase shift and the available bandwidth. Recent results include  $\sim 200^\circ$  phase shift at 1 GHz modulation frequency in a 2.5mm quantum well Semiconductor Optical Amplifier (SOA) [10] and  $\sim 120^\circ$  phase shift at 4 GHz in two SOA-EA (electroabsorber) pairs [14]. Recently, we reported a novel scheme based on optical filtering of the signal after transmission in an SOA, which strongly enhances the phase shift measured after photodetection and increases the available bandwidth [15]. In that work, the input optical signal with double sidebands was generated by a nearly chirp-free modulation and  $\sim 150^\circ$  phase delay at 19 GHz was achieved by blocking the red-shifted sideband using a fiber Bragg grating (FBG) notch filter after the SOA. Furthermore, at the same time the available slow light bandwidth was improved from a few GHz to 15 GHz.

In most experiments and theoretical analyses presented so far the phases of the sidebands of the input signal are implicitly assumed to correspond to that of a pure intensity modulated signal, also denoted as chirp-free. In this paper, we show that the chirp of the input signal plays an important role in the case of filtering-assisted slow and fast light schemes. We experimentally demonstrate that for the specific case of blocking the red-shifted sideband before detection, both  $\sim 120^\circ$  phase delay and  $\sim 170^\circ$  phase advance can be achieved by choosing different values of the initial chirp. The experimental results are shown to agree well with numerical simulations and can be qualitatively explained using an analytical perturbation approach.

## 2. Theory

Slow and fast light effects in semiconductor devices can be explained by the effect of Coherent Population Oscillations (CPO) [2] and can be described within the framework of four-wave mixing [7, 16]. In most cases, the input optical signal is created by intensity modulation of a single-frequency CW laser, the sidebands,  $E_{-1}$  and  $E_{+1}$ , and carrier,  $E_0$ , of which act as probe and pump beams, respectively [17]. For the case of small signal modulation, in the experiments reported here the power of the carrier is 20dB larger than that of the sidebands  $|E_0|^2 \gg |E_{+1}|^2$  and  $|E_{-1}|^2$ , the propagation equations for these electrical fields are:

$$\begin{cases}
\frac{\partial E_0}{\partial z} = \gamma_0 E_0 \\
\frac{\partial E_{-1}}{\partial z} = \gamma_0 E_{-1} + \xi_{-1} \left[ |E_0|^2 E_{-1} + E_0^2 E_{+1}^* \right] \\
\frac{\partial E_{+1}}{\partial z} = \gamma_0 E_{+1} + \xi_{+1} \left[ |E_0|^2 E_{+1} + E_0^2 E_{-1}^* \right]
\end{cases} \quad (1)$$

$$\gamma_0 = \frac{1}{2} [g_{sat} (1 - i\alpha) - a], \quad g_{sat} = \frac{\Gamma g_0}{1 + S}, \quad S = \frac{|E_0|^2}{P_{sat}}, \quad \text{and}$$

$$\xi_{\pm 1} = -\frac{1}{2} \frac{g_{sat}}{P_{sat}} \frac{1 + S \pm \alpha \Omega \tau_s - i\alpha(1 + S) \pm i\Omega \tau_s}{(1 + S)^2 + (\Omega \tau_s)^2}$$

where  $\Gamma g_0$  is the linear gain,  $\alpha$  is the linewidth enhancement factor,  $a$  is the internal loss,  $\Omega$  is the modulation frequency,  $P_{sat}$  is the saturation power,  $S$  is the normalized optical intensity, and  $\tau_s$  is the carrier lifetime.

After the SOA, the signal detected by a photo-detector is described as:

$$P_D \equiv P_0 + \left[ (P_{+1} + P_{-1}) e^{-i\Omega t} + c.c. \right]$$

Here we have introduced:

$$P_0 \equiv |E_0|^2, \quad P_{+1} \equiv E_0^* E_{+1}, \quad P_{-1} \equiv E_{-1}^* E_0, \quad \text{and} \quad P_{+1} + P_{-1} \equiv P \quad (2)$$

$P_{+1}$ ,  $P_{-1}$ , and  $P$  correspond, respectively, to the modulated part of the detected signal after the SOA when blocking the red-shifted sideband  $E_{-1}$ , blocking the blue-shifted sideband  $E_{+1}$ , or without optical filtering. From Eqs. (1) and (2) we may derive the following equation describing the evolution of the DC signal  $P_0$  and AC signals  $P$ ,  $P_{+1}$  and  $P_{-1}$ , the phases of which will contain the information of slow and fast light effects:

$$\begin{cases}
\frac{dP_0}{dz} = (\gamma_0 + \gamma_0^*) P_0 \\
\frac{dP}{dz} = (\gamma_0 + \gamma_0^*) P + (\xi_{+1} + \xi_{-1}^*) P_0 P \\
\frac{dP_{+1}}{dz} = (\gamma_0 + \gamma_0^*) P_{+1} + \xi_{+1} P_0 P \\
\frac{dP_{-1}}{dz} = (\gamma_0 + \gamma_0^*) P_{-1} + \xi_{-1}^* P_0 P
\end{cases} \quad (3)$$

In general, slow-down or speed-up of a signal centered at the probe frequency corresponds to a positive or negative dispersion of the refractive index seen by the probe with respect to the detuning frequency between the pump and the probe. However, in this paper, all results are obtained based on a technique of modulation. Therefore the signal is composed of three discrete optical frequencies, and the group refractive index can be substituted by the modulation refractive index as described in [17] and [7]. In this paper, slow or fast light will refer to whether the phase shift of the modulation relative to a reference phase is positive or negative, when the input optical power or the injection current is increased from a low value.

In [15], we have demonstrated that the phase shift of  $P_{+1}$  can be strongly enhanced for a nearly chirp-free input optical signal. Now if taking into account the initial modulation chirp of the input signal, the input electrical fields can be expressed as

$$\begin{cases} E_0(0) = |E_0(0)| \exp(i\theta_0) \\ E_{+1}(0) = E_{-1}(0) = |E_{+1}(0)| \exp(i\theta_1) \end{cases} \quad (4)$$

By combining Eqs. (2) and (4),

$$\begin{cases} P(0) = 2|E_0(0)E_{+1}(0)| \cos(\Delta\theta) \\ P_{+1}(0) = |E_0(0)E_{+1}(0)| [\cos(\Delta\theta) + i \sin(\Delta\theta)] \\ P_{-1}(0) = |E_0(0)E_{+1}(0)| [\cos(\Delta\theta) - i \sin(\Delta\theta)] \end{cases} \quad (5)$$

where  $\Delta\theta = \theta_1 - \theta_0$  is the initial optical phase difference between the carrier and sidebands, and reflects the degree of the modulation chirp of the input signal [18]. Based on Eq. (3) and the initial conditions expressed by Eq. (5), we can calculate the initial chirp dependence of the phase shifts. In this paper, all phase shifts are optically induced by changing the input optical power, but similar results can be obtained by considering a constant input power and changing the injection current of the SOA.

Figure 1 depicts the calculated phase shifts as a function of  $\Delta\theta$ . For each  $\Delta\theta$ , the phase shift occurs upon increasing the normalized input optical power  $S$  from 0.01 to 1.6, which corresponds to an absolute power change from -10dBm to 12dBm. The following main parameters are used:  $P_{sat} = 10\text{dBm}$ ,  $\tau_s = 100\text{ps}$ ,  $g_0 = 1.15 \times 10^4 \text{m}^{-1}$ ,  $\alpha = 6$ ,  $\Omega = 19\text{GHz}$  and the length of the SOA  $L = 500\mu\text{m}$ .

For the conventional case without optical filtering, represented by the variable  $P$ , it is easy to infer from Eq. (3) that the phase of  $P$  will not depend on  $\Delta\theta$ . This corresponds to the black curve in Fig. 1, showing a constant phase shift of  $-13.8^\circ$ . If the red-shifted sideband is blocked after propagation in the SOA, the blue curve in Fig. 1 shows that the final phase shift greatly depends on  $\Delta\theta$ . When  $-10^\circ \leq \Delta\theta < 90^\circ$ , a phase delay is induced by the slow light effect. At  $\Delta\theta = 0^\circ$ , corresponding to chirp-free modulation, a  $150^\circ$  phase shift is achieved [15]. On the other hand, a phase advance is observed for  $90^\circ < \Delta\theta \leq 170^\circ$ . As  $\Delta\theta$  approaches  $90^\circ$  from either side, the absolute value of the phase shift will vanish. Notice that  $\Delta\theta = 90^\circ$  corresponds to a pure phase modulated input signal, for which there is no amplitude modulation of the detected signal. When the blue-shifted sideband is blocked, the final phase shift will depend slightly on  $\Delta\theta$ , as shown by the red curve in Fig. 1. Thus, as  $\Delta\theta$  increases from  $-10^\circ$  to  $90^\circ$ , the numerical value of the phase advance will increase from  $-21.1^\circ$  and even flip into a phase delay of  $6^\circ$  at  $\Delta\theta = 76^\circ$ . If  $\Delta\theta$  increases continuously from  $90^\circ$  to  $170^\circ$ , there will be a maximum phase advance of  $-37.6^\circ$ , achieved at  $\Delta\theta = 126^\circ$ .

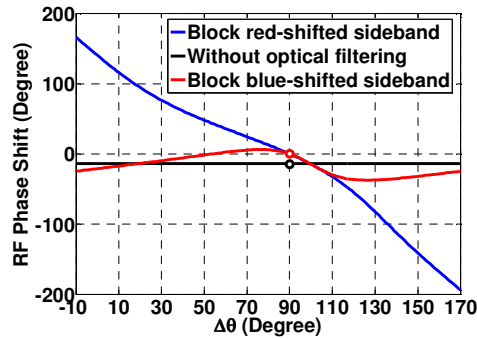


Fig. 1. Calculated RF phase shifts of  $P$  (black),  $P_{+1}$  (blue) and  $P_{-1}$  (red) induced by changing the normalized input optical power  $S$  from 0.01 to 1.6 as a function of the chirp parameter  $\Delta\theta$  indicating the initial phase difference.

### 3. Experimental set-up and results

Figure 2(a) shows the experimental set-up. To achieve a tunable chirp  $\Delta\theta$ , the input optical signal with two sidebands was generated by modulating a CW laser beam, at a wavelength of 1539.5nm, using a Dual-Arm Mach-Zehnder Modulator (DA-MZM), where only one arm is biased and modulated at 19GHz. The chirp of the DA-MZM can be changed by the bias voltage [19] and the output electrical fields from the DA-MZM can be derived:

$$\begin{cases} E_0(0) = \frac{A}{2} \left[ 1 + \exp(-i \frac{V_{DC}}{V_\pi} \pi) J_0(\frac{V}{V_\pi} \pi) \right] \equiv |E_0(0)| \exp(i\theta_0) \\ E_{+1}(0) = i \frac{A}{2} \exp(-i \frac{V_{DC}}{V_\pi} \pi) J_{+1}(\frac{V}{V_\pi} \pi) \equiv |E_{+1}(0)| \exp(i\theta_1) \\ E_{-1}(0) = -i \frac{A}{2} \exp(-i \frac{V_{DC}}{V_\pi} \pi) J_{-1}(\frac{V}{V_\pi} \pi) \equiv |E_{-1}(0)| \exp(i\theta_1) \end{cases} \quad (6)$$

Here,  $V=0.3V$ ,  $V_{DC}$ , and  $V_\pi=3.9V$  are the peak voltage of the modulation signal, the bias voltage and the half-wave voltage, respectively. According to Eq. (6)  $\Delta\theta$  ( $=\theta_1-\theta_0$ ) can be altered between  $0^\circ$  and  $180^\circ$  by changing the bias voltage  $V_{DC}$ , as shown by the blue lines in Fig. 2(b). To avoid double-frequency modulation, the DA-MZM should not be biased in the gray shaded areas, which restricts the available range of  $\Delta\theta$ , to the range  $20^\circ < \Delta\theta < 80^\circ$  and  $110^\circ < \Delta\theta < 160^\circ$ . After the SOA, the signal passes through a tunable FBG notch filter with a bandwidth of 0.1nm before being detected by the network analyzer [15]. The input optical power can be adjusted between -10dBm and 12dBm via an Erbium Doped Fiber Amplifier (EDFA) and a variable optical attenuator (VOA).

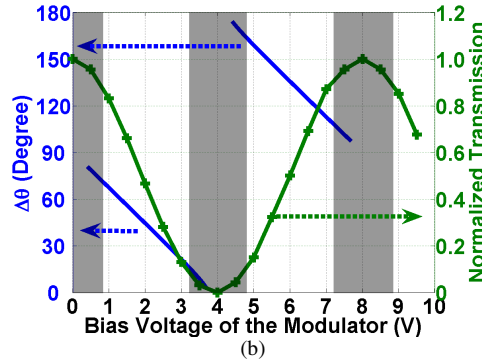
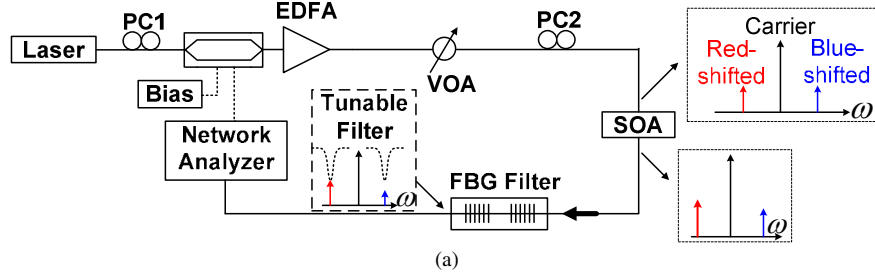


Fig. 2. (a) Experimental set-up. (b) The green line shows the measured transmission curve of the DA-MZM. The blue lines show the corresponding initial optical phase difference  $\Delta\theta$ , calculated using Eq. (6), as a function of the bias voltage.

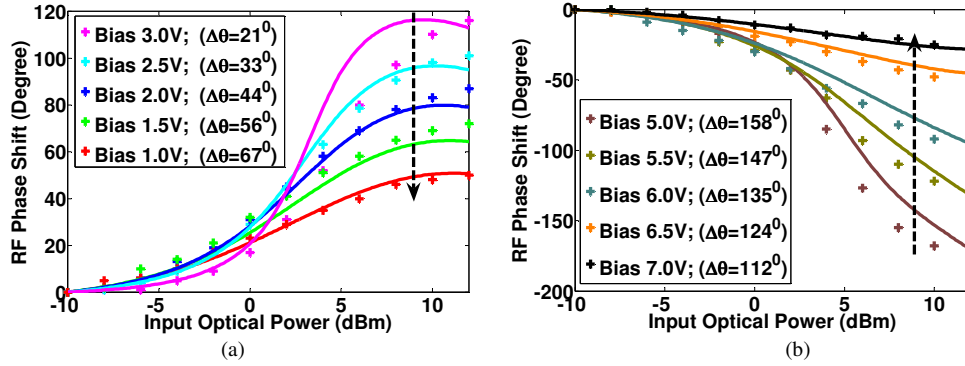


Fig. 3. Measured (markers) and simulated (solid lines) RF phase shifts of the detected microwave modulation as a function of the input optical power for different values of the initial chirp, realized by changing the bias voltages of the DA-MZM. In all cases the red-shifted sideband is blocked before detection. (a)  $21^\circ \leq \Delta\theta \leq 67^\circ$  and (b)  $112^\circ \leq \Delta\theta \leq 158^\circ$ . The reference phase is chosen at the input optical power of -10dBm for each of the bias voltages.

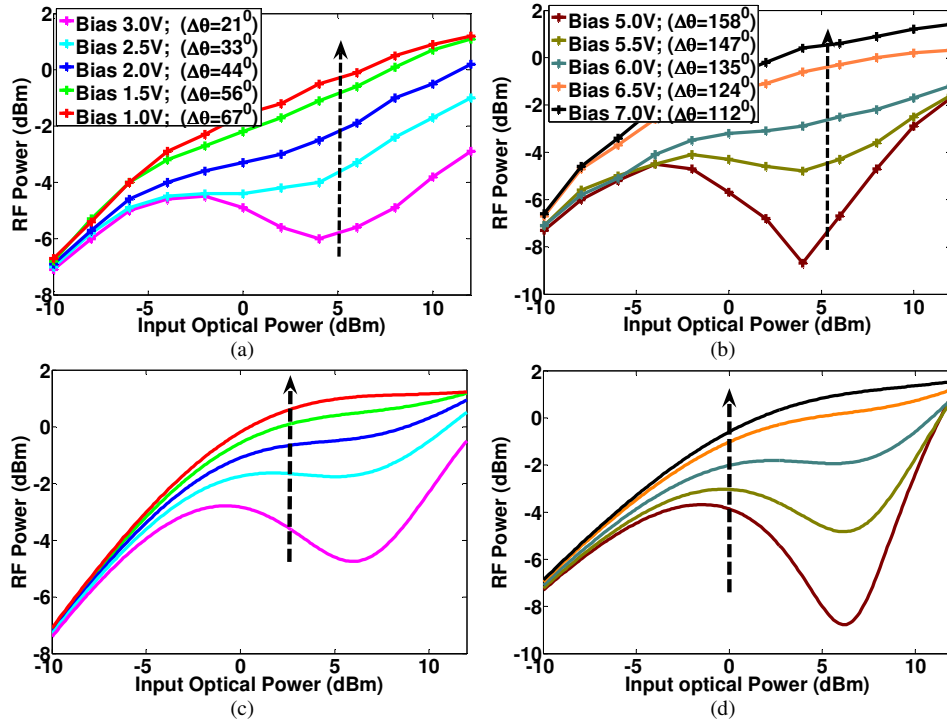


Fig. 4. Measured RF power versus input optical power for (a)  $21^\circ \leq \Delta\theta \leq 67^\circ$  and (b)  $112^\circ \leq \Delta\theta \leq 158^\circ$ . (c) and (d) show the corresponding simulated results for the same values of the chirp parameter. In all cases the red-shifted sideband is blocked before detection.

Figure 3 shows the measured RF phase shifts (markers) versus input optical power for different values of the chirp parameter  $\Delta\theta$  (bias voltages of the DA-MZM) for the case where the red-shifted sideband is blocked before the detection. During the measurement, the SOA is operated at a constant current of 160 mA. From Fig. 3(a), a positive phase shift (slow light) is obtained for  $21^\circ < \Delta\theta < 67^\circ$ . The maximum phase shift decreases as  $\Delta\theta$  increases from  $21^\circ$  to  $67^\circ$ . If the DA-MZM is biased at a higher voltage than  $V_{\pi}$ , a negative phase shift, corresponding to fast light is achieved. The maximum obtained phase advance decreases as  $\Delta\theta$  decreases from  $158^\circ$  to  $112^\circ$ . The measured initial chirp dependence of the phase shift thus

shows a good agreement with the numerical simulations in Fig. 1, which are calculated using the parameters in section 2 and the description of four-wave mixing expressed by Eqs. (3) and (5). However, at low input optical power levels, e.g. -4dBm, the RF phase shift does not monotonously decrease for increasing  $\Delta\theta$ . Figure 3(a) and (b) show the maximum values of the absolute RF phase shift at  $\Delta\theta=44^\circ$  and  $\Delta\theta=135^\circ$ , respectively. These RF phase variations at low input optical power can be understood by the perturbation theory presented in section 4.

Figure 4 gives the RF power changes corresponding to Fig. 3. Figures 4(a) and 4(b) are measured results. In both cases,  $21^\circ \leq \Delta\theta \leq 67^\circ$  and  $112^\circ \leq \Delta\theta \leq 158^\circ$ , the magnitude of the RF power dip decreases as the absolute RF phase shift decreases. The power dip contributes to the sharp RF phase change [15]. Figures 4(c) and 4(d) are calculated curves in good agreement with the experimental results. These 5~10 dB RF power variations could be a limitation for a real microwave photonic application [6].

If the blue-shifted sideband is filtered away before detection, the maximum phase advance decreases from  $15^\circ$  to  $4^\circ$  when  $\Delta\theta$  increases from  $21^\circ$  to  $67^\circ$ , and a small phase delay is observed at  $\Delta\theta=67^\circ$  when the input optical power is around 0dBm, as shown in Fig. 5(a). If  $\Delta\theta$  increases further, a larger phase delay is expected. However, this parameter range cannot be accessed in the present experiment due to the strong double-frequency modulation at the required bias voltages, cf. gray areas in Fig. 2(b). On the other hand, when  $\Delta\theta$  decreases from  $158^\circ$  to  $124^\circ$ , the phase advance increases from  $25^\circ$  to  $35^\circ$ , shown in Fig. 5(b). These measured phase changes also agree well with the red line in Fig. 1.

As for the conventional case in Fig. 5(c), without optical filtering, a  $\sim 17^\circ$  phase advance is obtained independently of the values of the initial chirp.

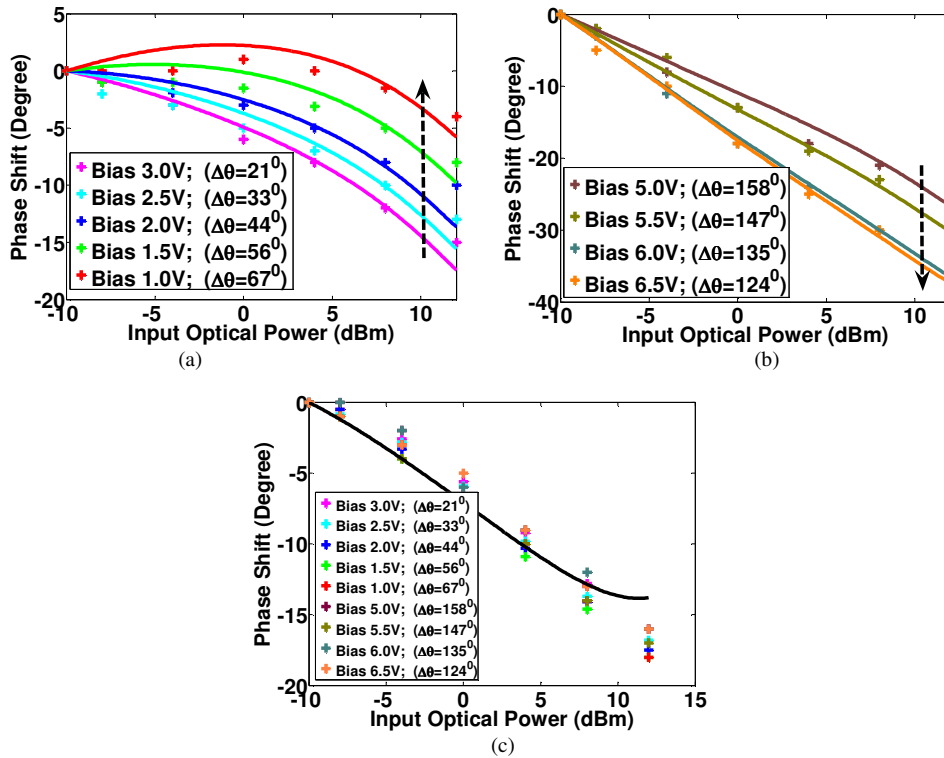


Fig. 5. Measured (markers) and simulated (solid lines) phase shifts of the detected microwave modulation as a function of input optical power for different bias voltages of the DA-MZM. (a)  $21^\circ \leq \Delta\theta \leq 67^\circ$  and (b)  $124^\circ \leq \Delta\theta \leq 158^\circ$  are for the case of blocking the blue-shifted sideband and (c) is without optical filtering.



#### 4. Discussion

The results presented above can be qualitatively understood by the use of an approximate analytical perturbation theory that elucidates the roles of the various effects that contribute to the phase shift. Because of the significant enhancements of the phase shift seen when blocking the red-shifted sideband, which is potentially interesting for many applications, we will here focus on this case. For small propagation distances  $\delta L$  in the SOA, the propagation effect on the saturation induced by the DC field can be neglected. Starting with Eqs. (3) and (5) and using the same method as in [15], the output  $P$ ,  $P_{+1}$  and  $P_{-1}$  from the SOA can be approximately derived:

$$\begin{aligned} P(\delta L) &= P(0) + \Delta P \\ &= 2|E_0 E_1| \cos(\Delta\theta) \left[ 1 + (g_{sat} - a + \gamma_1)\delta L + i\beta_1 \delta L \right] \end{aligned} \quad (7a)$$

$$\begin{aligned} P_{+1}(\delta L) &= P_{+1}(0) + \Delta P_{+1} \\ &= |E_0 E_1| \cos \Delta\theta \left\{ \left[ 1 + (g_{sat} - a + \gamma_1 + \alpha\beta_1)\delta L \right] + \right. \\ &\quad \left. i \left[ \tan \Delta\theta + (\beta_1 - \alpha\gamma_1 + (g_{sat} - a) \tan \Delta\theta) \delta L \right] \right\} \end{aligned} \quad (7b)$$

$$\begin{aligned} P_{-1}(\delta L) &= P_{-1}(0) + \Delta P_{-1} \\ &= |E_0 E_1| \cos(\Delta\theta) \left\{ \left[ 1 + (g_{sat} - a + \gamma_1 - \alpha\beta_1)\delta L \right] + \right. \\ &\quad \left. i \left[ -\tan(\Delta\theta) + [\beta_1 + \alpha\gamma_1 - (g_{sat} - a) \tan(\Delta\theta)] \delta L \right] \right\} \end{aligned} \quad (7c)$$

where

$$\begin{aligned} \gamma_1 &= -g_{sat} \frac{(1+S)S}{(1+S)^2 + (\Omega\tau_s)^2} \\ \beta_1 &= -g_{sat} \frac{\Omega\tau_s S}{(1+S)^2 + (\Omega\tau_s)^2} \end{aligned}$$

For the conventional case, without optical filtering, from Eq. (7a), it is easy to see that the phase shift of  $P$  does not depend on  $\Delta\theta$ . For the case when the red-shifted sideband is blocked, we illustrate  $P_{+1}(\delta L)$  in the complex plane in Fig. 6(a). If the input signal is chirped, we have  $\Delta\theta$  different from  $0^\circ$ . The initial position of  $P_{+1}(\delta L)$ , illustrated by thick black arrows in Fig. 6(a), will then have an angle of  $\Delta\theta$  with respect to the real ( $Re$ ) axis. From Eq. (7b), the approximate analytical phase shift  $\delta\varphi_{+1}(\delta L)$ , induced by increasing the input optical power, then becomes:

$$\begin{aligned} \delta\varphi_{+1}(\delta L) &= \arg\{P_{+1}(\delta L)\}_S - \arg\{P_{+1}(\delta L)\}_{S_{ref}} \\ &\approx \arctan\{\cos^2(\Delta\theta)[\beta_1 - \alpha\gamma_1 - (\gamma_1 + \alpha\beta_1) \tan(\Delta\theta)]\delta L\} \end{aligned} \quad (8)$$

For a very short propagation distance in the SOA, Eq. (8) demonstrates that the phase shift  $\delta\varphi_{+1}(\delta L)$ , strongly depends on  $\Delta\theta$ . From Eq. (8), the phase shift vanishes,  $\delta\varphi_{+1}(\delta L)=0$ , when  $\Delta\theta$  satisfies

$$\cos(\Delta\theta) = 0 \Rightarrow \Delta\theta = \pm 90^\circ \quad (9a)$$

$$\text{or} \quad \tan(\Delta\theta) = \frac{\beta_1 - \alpha\gamma_1}{\gamma_1 + \alpha\beta_1} \quad (9b)$$

Equation (9a) corresponds to the condition for a purely phase modulated signal, i.e., there is no intensity modulation of the input optical signal. According to Eq. (9b), the value of the chirp parameter depends on the normalized input optical power,  $\alpha$  factor, carrier recovery

time, and modulation frequency. Using the parameters of section 2,  $\Delta\theta$  will equal  $-10^\circ$  or  $170^\circ$ . Both phase delay  $\delta\varphi_{+j}(\delta L) > 0$  and phase advance  $\delta\varphi_{+j}(\delta L) < 0$  can be obtained for  $90^\circ > \Delta\theta \geq -10^\circ$  and  $170^\circ \geq \Delta\theta > 90^\circ$ , respectively, as shown in Fig. 6(b). Therefore  $P_{+j}(\delta L)$  will always rotate towards the imaginary ( $Im$ ) axis, as illustrated by the blue dotted arrows in Fig. 6(a).

Compared with Eq. (7c), derived for the case where the blue-shifted sideband is blocked, the absolute value of the real part of Eq. (7b) decreases, rather than increases, as the input optical power increases. This means that a larger phase shift is expected when blocking the red-shifted sideband rather than the blue-shifted sideband before detection [15]. These results are in good agreement with a more extensive model but without taking into account the effects of the generation of the conjugate waves [7, 20]. For the limiting case of a very short length of the SOA, the generation of the conjugate wave can be neglected. The refractive index experienced by the sideband (probe) is modified asymmetrically by the carrier (pump) due to the nonzero linewidth enhancement factor  $\alpha$ . Therefore, the blue-shifted sideband will experience a larger group refractive index than the red-shifted sideband.

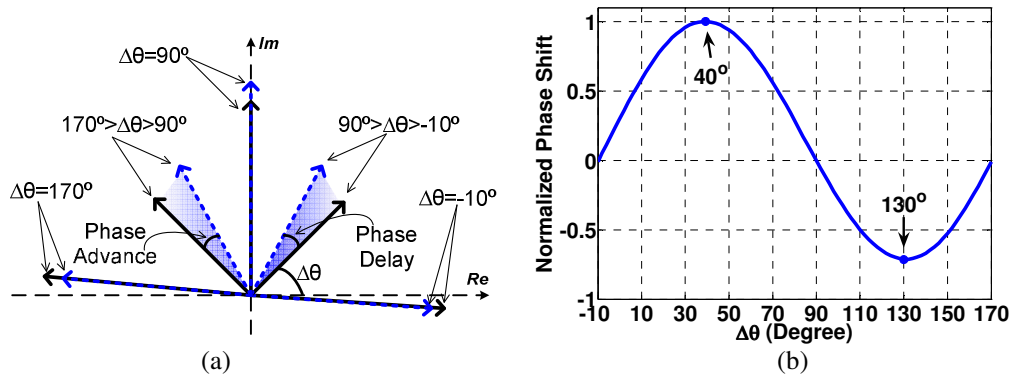


Fig. 6. (a). Representation of the complex power  $P_{+j}(\delta L)$  in the complex plane for different values of the initial phase difference  $\Delta\theta$ . The thick black arrows indicate the reference points corresponding to minimum input optical power. Upon increasing the power the arrows rotate towards the dotted blue arrows, which correspond to the maximum input optical power. (b). The normalized phase shift  $\delta\varphi_{+j}(\delta L)$  as a function of  $\Delta\theta$  (the length of the SOA is  $10\ \mu\text{m}$ ).

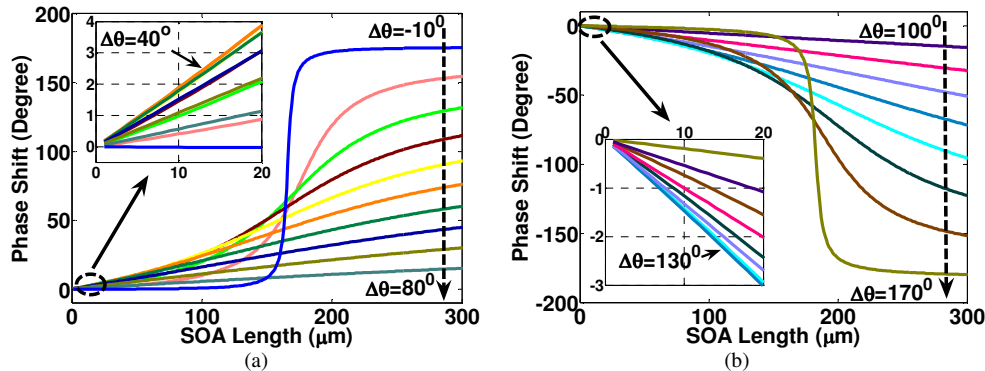


Fig. 7. Calculated phase shifts of  $P_{+j}$  induced by increasing  $S$  from 0.01 to 1.6 as a function of the SOA length for (a)  $-10^\circ < \Delta\theta < 90^\circ$  and (b)  $90^\circ < \Delta\theta < 170^\circ$ . (The increment between curves is  $10^\circ$ )

As the SOA length increases, saturation and propagation effects have to be properly included. We find that the generation of the conjugate wave by the FWM effect will strongly influence the propagation of the probe itself, making a simple analysis unfeasible. Full numerical calculations of the phase shift of  $P_{+j}$  as a function of SOA length are shown in Fig. 7. When the SOA is short, as  $\Delta\theta$  increases the absolute phase shift firstly increases until

reaching a maximum at  $\Delta\theta \approx 40^\circ/130^\circ$ , and then decreases in both the slow-down regime, as shown by the inset in Fig. 7(a), and speed-up regime, as shown by the inset in Fig. 7(b). These numerical simulations show a good agreement with above perturbation theory in Fig. 6(b). If the SOA is long enough, the phase shift of  $P_{+j}$  will monotonously decrease from  $175^\circ$  to  $-180^\circ$  as  $\Delta\theta$  increases from  $-10^\circ$  to  $170^\circ$ .

## 5. Conclusion

We have experimentally demonstrated that the phase shift induced by slow and fast light effects in semiconductor optical amplifiers strongly depends on the initial modulation chirp in schemes where optical filtering is used before detection. By using different values of the input modulation chirp,  $\sim 120^\circ$  phase delay as well as  $\sim 170^\circ$  phase advance at 19 GHz has been realized by changing the input optical power. Numerical simulations based on a four-wave mixing model show good agreement with the experimental results. Furthermore, a simple perturbative analysis provides good insight into the physical effects at play. This characteristic of the initial chirp dependence provides a possible way to combine  $\sim 120^\circ$  phase delay and  $\sim 170^\circ$  phase advance for achieving tunable  $\sim 360^\circ$  phase shifters at high modulation frequency. This is highly desired for many applications in microwave photonics, such as microwave photonic filters [21]. Because this scheme cannot, in its present form, provide a linear frequency dependence of the RF phase shift [15], also known as true time delay, it might have limited applicability to wideband phased array antennas, but may rather be interesting for narrowband applications [14].

## Acknowledgment

The authors would like to acknowledge financial support from the Danish Research Councils through the QUEST project as well as from FET programme (FP7 for Research of the European Commission) under FET-Open grant no. 219299 ("GOSPEL"). The authors thank Prof. Salvador Sales at Universidad Polit cnica de Valencia for the helpful discussions and providing FBG notch filters.